

# MICINet: Multi-Level Inter-Class Confusing Information Removal for Reliable Multimodal Classification

Tong Zhang, Shu Shen, C. L. Philip Chen

**Abstract**—Reliable multimodal learning in the presence of noisy data is a widely concerned issue, especially in safety-critical applications. Many reliable multimodal methods delve into addressing modality-specific or cross-modality noise. However, they fail to handle the coexistence of both types of noise efficiently. Moreover, the lack of comprehensive consideration for noise at both global and individual levels limits their reliability. To address these issues, a reliable multimodal classification method dubbed Multi-Level Inter-Class Confusing Information Removal Network (MICINet) is proposed. MICINet achieves the reliable removal of both types of noise by unifying them into the concept of Inter-class Confusing Information (*ICI*) and eliminating it at both global and individual levels. Specifically, MICINet first reliably learns the global *ICI* distribution through the proposed *Global ICI Learning Module*. Then, it introduces the *Global-guided Sample ICI Learning module* to efficiently remove global-level *ICI* from sample features utilizing the learned global *ICI* distribution. Subsequently, the *Sample-adaptive Cross-modality Information Compensation module* is designed to remove individual-level *ICI* from each sample reliably. This is achieved through interpretable cross-modality information compensation based on the complementary relationship between discriminative features and *ICI* and the perception of the relative quality of modalities introduced by the relative discriminative power. Experiments on four datasets demonstrate that MICINet outperforms other state-of-the-art reliable multimodal classification methods under various noise conditions. MICINet achieves up to 7.2% improvement in ACC, 6.6% in Weighted F1, and 14.9% in Macro F1 on multi-class datasets, and up to 7.2% in ACC, 5.9% in F1, and 4.9% in AUC on binary classification dataset.

**Index Terms**—Multimodal classification, modality-specific noise, cross-modality noise, reliable multimodal classification.

## I. INTRODUCTION

WITH the rapid advancement of various sensors, multimodal data is readily accessible and widely used to enhance the performance of different applications. For example, single-cell multimodal sequencing technologies [1]–[4] utilizing information from multiple modalities such as DNA, mRNA, and miRNA to achieve comprehensive analyses of cells. Autonomous driving systems achieve safer operations by integrating data from various sensors [5]–[9]. However, multimodal data often contains noise, significantly reducing the reliability of multimodal classification, a critical issue in safety-critical applications such as medicine, finance, and autonomous driving. Regarding the type, multimodal noise can be categorized into modality-specific and cross-modal noise [10]. The former refers to noise introduced into each modality’s data due to sensor malfunction, environmental impact, or transmission errors. The latter refers to weakly aligned

or unaligned multimodal samples [11], [12]. Regarding the characteristics, multimodal noise can be classified into global-level noise, such as sensor errors that introduce consistently distributed noise across all samples, and individual-level noise, such as misalignment in a particular sample due to data collection errors.

In real-world scenarios, data is often contaminated by both modality-specific and cross-modal noise simultaneously (e.g., misaligned data encountering transmission errors). However, existing methods typically focus on addressing only one type of noise and fail to handle cases where both types coexist effectively. Many methods effectively remove modality-specific noise based on confidence of each modality [13]–[20]. However, they are weak in identifying or realigning misaligned samples, thus failing to address cross-modality noise. In contrast, numerous methods are dedicated to addressing misaligned samples [21]–[28]. These methods employ specially designed rules, models, or regularizations to filter out, rectify, or reduce the impact of misaligned samples on the model. However, the presence of modality-specific noise severely impairs the ability of these methods to discern and learn the alignment relationships between modalities. Moreover, the above-mentioned methods generally fail to address global-level and individual-level noise concurrently, thereby limiting the reliability of noise removal. Among them, [16], [18]–[26] focus on individual-level noise removal while neglecting the learning of global-level noise. [15], [28] remove noise from a global perspective but overlook the dynamic quality of individual samples. Thus, an important question is raised: ***How to design a reliable multimodal classification method that simultaneously removes modality-specific and cross-modality noise at both global and individual levels?***

To address this question, a novel paradigm named Multi-Level Inter-Class Confusing Information Removal Network (MICINet) is designed. MICINet simultaneously removes both types of noise by unifying them under the concept of Inter-class Confusing Information (*ICI*) and reliably eliminating it at both global and individual levels. *ICI* is proposed based on the observation that two types of noise both introduce useless or erroneous information that leads to classification confusion. It can be intuitively learned by extracting and aggregating the shared information between different class pairs. While learning and removing *ICI*, MICINet fully considers it at both the global and individual levels and delves into their characteristics. At the global level, MICINet observes the variation of *ICI* distributions and degrees of confusion among

different class pairs. For individual *ICI*, MICINet notes that it leads to varying information incompleteness and quality across modalities in different samples. Based on these findings, a two-stage pipeline for reliable global and individual *ICI* removals is established.

Specifically, in the first stage, MICINet focuses on global *ICI* removal. The **Global *ICI* Learning module (GICI)** is first introduced to learn the global *ICI* distribution of the data. A novel dual-path structure is proposed to extract the shared information between any two classes as their *ICI* distribution and estimate their confusion degree. It then employs the learned *ICI* distribution and confusion degree of different class pairs to construct a Gaussian Mixture Model (GMM) for modeling the global *ICI* distribution. Subsequently, the **Global-Guided Sample *ICI* Learning module (SICI)** achieves reliable global-level *ICI* removal for each sample by pushing the extracted discriminative features of each modality away from the global *ICI* distribution. In the second stage, the individual *ICI* is further eliminated via the proposed **Sample-Adaptive Cross-Modality Information Compensation module (CMIC)**. **CMIC** first performs an interpretable cross-modality compensatory information query by exploiting the complementary relationship between discriminative features and *ICI*. Concretely, for each modality, its *ICI* is used to obtain information from the discriminative features of other modalities via an attention mechanism. Then, the relative discriminative power is adopted to reliably integrate the obtained information from all other modalities based on their relative qualities to compensate for the information incompleteness of each modality.

The contributions of this paper can be summarized as:

- The proposed MICINet is the first method to address the scenario where modality-specific and cross-modality noise coexist. Both types of noise are unified and simultaneously removed under the proposed concept of Inter-class Confusing Information (*ICI*). Experiments show that MICINet significantly outperforms other state-of-the-art multimodal classification methods in accuracy and reliability under different noise settings.
- MICINet reliably removes *ICI* by comprehensively considering it at both the global and individual levels and establishing a two-stage removal pipeline based on their respective variable characteristics.
- A novel dual-path network is designed for global-level *ICI* learning by characterizing diverse *ICI* distributions and confusion degrees between different class pairs. An interpretable information compensation with relative quality estimation across modalities is proposed to reliably remove individual-level *ICI* based on the variable information incompleteness and quality of modalities across samples.

## II. RELATED WORKS

This section briefly reviews some related works on multimodal learning, modality-specific noise removal, and cross-modality noise removal.

### A. Multimodal Learning

Multimodal learning integrates information from different types of data, achieving effective representation learning with a wide range of applications in real-world scenarios [29]–[31]. Based on the fusion strategy, multimodal learning can be classified into early fusion [32], intermediate fusion [33]–[41], and decision fusion [42]–[45]. Early fusion directly integrates various modalities at the data level to utilize the correlation and interaction between low-level features [32]. Still, it cannot fully exploit the complementary between multiple modal data and may suffer from information redundancy. Intermediate fusion, widely adopted in multimodal learning, integrates modalities at the intermediate feature level, capturing the complementary relationships between high-level features of each modality [33]–[41]. Decision fusion, involves extracting features from each modality and obtaining predictions from individual classifiers for each modality, which are then integrated to obtain the final multi-modal prediction result [42]–[45].

### B. Modality-Specific Noise Removal

Many studies have developed reliable multimodal classification methods to remove modality-specific noise. Federici et al. [46] proposed the multi-view information bottleneck, which improved the generalization and robustness of multi-view learning by retaining information shared by each view. Han et al. [13] parameterized the evidence of different modality features using Dirichlet distribution and fused each modality at the evidence level using Dempster-Shafer theory. Geng et al. [15] proposed the DUA-Nets, which achieved uncertainty-based multimodal representation learning through reconstruction. Han et al. [16] modeled informativeness at the feature and modality levels, achieving trustworthy multimodal feature fusion. Zhang et al. [19] achieved more robust and generalized multimodal fusion by dynamically assigning weights to each modality based on uncertainty estimation. Zheng et al. [47] achieved trustworthy multimodal classification via integrating feature and label-level confidence. Zou et al. [18] proposed a novel dynamic poly-attention Network that integrated global structural information for trustworthy multimodal classification. Zhou et al. [17] introduced a trustworthy multi-view classification framework by enhancing multi-view encoding and confidence-aware fusion. Cao et al. [20] proposed the Predictive Dynamic Fusion method, which provides theoretical guarantees for reducing the upper bound of generalization error in dynamic multimodal fusion.

### C. Cross-Modality Noise Removal

Many studies have focused on identifying or realigning misaligned sample pairs or achieving reliable multimodal learning using incomplete sample pairs. These methods can be categorized into rules-based filtering, model-based rectifying, and noise-robust regularization. Rules-based filtering refers to methods for data cleaning through the design of a set of rules. Representative works include those by Radenovic et al. [21], Gadre et al. [48], and Sharma et al. [49]. Model-based rectifying methods design models to filter or rectify misaligned

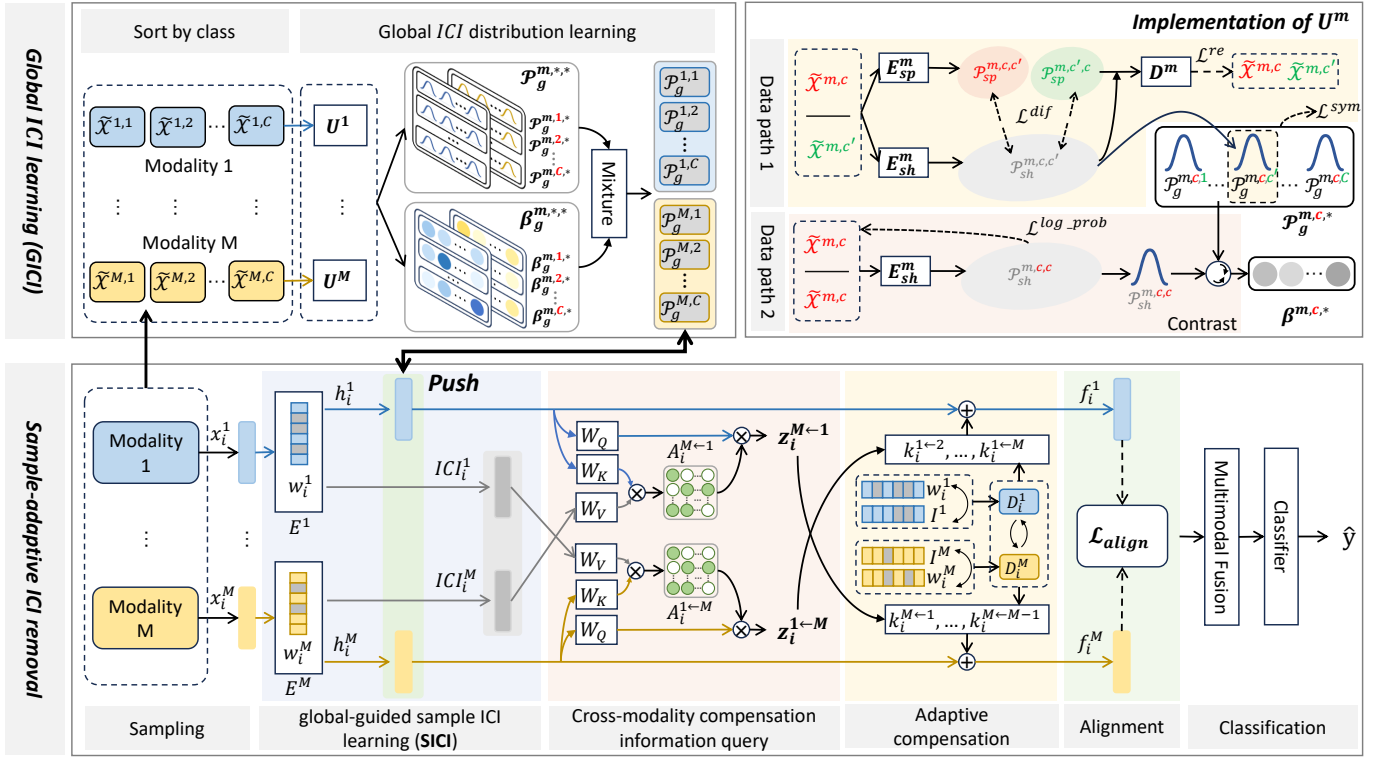


Fig. 1. The framework of the proposed Multi-Level Inter-Class Confusing Information Removal Network (MICINet).

samples, such as NCR [22], ALBEF [23], and BLIP [24]. Noise robust regularization methods mitigate the impact of misaligned samples on the model by designing regularization, such as NLP [25] and OSCAR [26]. Some studies also design reliable learning methods that do not rely on paired samples, such as SMILE [28].

### III. THE PROPOSED METHOD

#### A. Problem Definition

Given a dataset  $\mathcal{D} = (\mathcal{X}, \mathcal{Y})$  consists of  $N$  multimodal samples  $\mathcal{X} = \{x_i\}_{i=1}^N$  from  $C$  classes, along with their corresponding ground truth labels  $\mathcal{Y} = \{y_i \in \mathbb{R}^C\}_{i=1}^N$ . Each multimodal sample  $x_i = \{x_i^m \in \mathbb{R}^{d^m}\}_{m=1}^M$ ,  $i \in [1, N]$  contains samples from  $M$  modalities, where  $d^m$  is the dimension of the  $m$ -th modality. Multimodal classification methods aim to learn a neural network that maps each sample  $x_i$  to its corresponding class label  $y_i$ .

To remove both modality-specific and cross-modal noise in dataset  $\mathcal{D}$  for reliable classification, this paper proposes MICINet based on the concept of *ICI*. MICINet is a two-stage *ICI* removal pipeline. The first stage includes the global *ICI* learning (*GICI*) and global-guided sample *ICI* learning (*SICI*) modules, which are elaborated respectively in Section III-B and III-C. The second stage corresponds to the sample-adaptive cross-modality information compensation module (*CMIC*), which is detailed in Section III-D.

#### B. Global ICI Learning Module (*GICI*)

1) *Definition of Global ICI Distribution*: In this paper, the global *ICI* distribution in dataset  $\mathcal{D}$  is defined as

$\mathcal{P}_g = \{\{\mathcal{P}_g^{m,c}\}_{c=1}^C\}_{m=1}^M$ , where  $\mathcal{P}_g^{m,c} = \text{Mix}(\{\beta^{m,c,c'}\}_{c' \neq c}^C)$ .  $\mathcal{P}_g^{m,c,c'} \sim \mathcal{N}(\mu^{m,c,c'}, \sigma^{m,c,c'})$  refers to the distribution of confusing information between the  $c$ -th and the  $c'$ -th class of the  $m$ -th modality. It is obtained by extracting the shared information distribution between data of class  $c$  and  $c'$  in the  $m$ -th modality.  $\beta^{m,c,c'}$  refers to the confusion degree between class  $c$  and  $c'$  in the  $m$ -th modality. *Mix* represents the mixture of distributions of confusing information using their respective confusion degree.

2) *Overview of GICI*: *GICI* is proposed to extract the global *ICI* distribution  $\mathcal{P}_g$ . The learning of  $\mathcal{P}_g$  consists of two parts: the confusing information distribution  $\mathcal{P}_g^{m,c,c'}$  between any two classes within each modality and their corresponding confusion degree  $\beta^{m,c,c'}$ . Before learning, the input feature vectors of all samples  $\mathcal{X} = \{\{x_i^m\}_{m=1}^M\}_{i=1}^N$  are first organized according to different classes and modalities, yield  $\tilde{\mathcal{X}} = \{\{\tilde{\mathcal{X}}^{m,c}\}_{m=1}^M\}_{c=1}^C$ .  $\tilde{\mathcal{X}}^{m,c} = \{x_i^m\}_{i=1}^{N^{m,c}}$  contains the feature vectors of the  $m$ -th modality from all samples belonging to the  $c$ -th class.

*GICI* introduces  $M$  modality-specific network structures  $\{\mathbf{U}^m\}_{m=1}^M$  to learn  $\mathcal{P}_g$ . Each network  $\mathbf{U}^m$  employs a novel dual-path to learn the confusing information distribution and estimate the confusion degree between all class pairs within the corresponding modality  $m$ :

$$\{\{\mathcal{P}_g^{m,c,c'}\}_{c=1}^C\}_{c' \neq c}^C, \{\{\beta^{m,c,c'}\}_{c=1}^C\}_{c' \neq c}^C = \mathbf{U}^m(\{\tilde{\mathcal{X}}^{m,c}\}_{c=1}^C). \quad (1)$$

The global *ICI* distribution is then obtained by mixing the distributions  $\{\{\mathcal{P}_g^{m,c,c'}\}_{c=1}^C\}_{c' \neq c}^C$  with their corresponding weights  $\{\{\beta^{m,c,c'}\}_{c=1}^C\}_{c' \neq c}^C$  in each modality. The following

paragraphs will introduce the detailed implementation of each network structure  $\mathbf{U}^m$ .

3) *Detailed Implementation of  $\mathbf{U}^m$* : As demonstrated in Figure 1,  $\mathbf{U}^m$  consists of two encoders  $\mathbf{E}_{sp}^m, \mathbf{E}_{sh}^m$ , and a decoder  $\mathbf{D}$ . Both encoders receive inputs from two batches of samples simultaneously. Encoder  $\mathbf{E}_{sp}^m$  learns the specific information of each batch relative to the other, while encoder  $\mathbf{E}_{sh}^m$  learns the shared information between the two batches. The decoder  $\mathbf{D}$  merges the specific and shared information of each batch and reconstructs it, thereby guiding the model's learning.

$\mathbf{U}^m$  contains two separate data paths (dual-path). The first data path takes two batches of samples from different classes  $c$  and  $c'$ , i.e.,  $\tilde{\mathcal{X}}^{m,c}$  and  $\tilde{\mathcal{X}}^{m,c'}$  together as input. The encoder  $\mathbf{E}_{sp}^m$  learns the specific information  $\mathcal{P}_{sp}^{m,c,c'}$  of class  $c$  relative to class  $c'$ , and the specific information  $\mathcal{P}_{sp}^{m,c',c}$  of class  $c'$  relative to class  $c$ :  $\mathcal{P}_{sp}^{m,c,c'}, \mathcal{P}_{sp}^{m,c',c} = \mathbf{E}_{sp}^m(\tilde{\mathcal{X}}^{m,c} \oplus \tilde{\mathcal{X}}^{m,c'})$ . The encoder  $\mathbf{E}_{sh}^m$  learns the shared information  $\mathcal{P}_{sh}^{m,c,c'}$  between two classes:  $\mathcal{P}_{sh}^{m,c,c'} = \mathbf{E}_{sh}^m(\tilde{\mathcal{X}}^{m,c} \oplus \tilde{\mathcal{X}}^{m,c'})$ . The shared information distribution  $\mathcal{P}_{sh}^{m,c,c'}$  between  $c$  and  $c'$  is the desired *ICI* distribution  $\mathcal{P}_g^{m,c,c'}$  between them:

$$\mathcal{P}_g^{m,c,c'} = \mathcal{P}_{sh}^{m,c,c'}. \quad (2)$$

The second data path takes two batches of samples from the same class  $c$  together as input and computes using only the encoder  $\mathbf{E}_{sh}^m$ , resulting in a probability distribution  $\mathcal{P}_{sh}^{m,c,c}$ :  $\mathcal{P}_{sh}^{m,c,c} = \mathbf{E}_{sh}^m(\tilde{\mathcal{X}}^{m,c} \oplus \tilde{\mathcal{X}}^{m,c})$ . Subsequently, the confusion degree between class  $c$  and other classes  $c'$ :  $\{\beta^{m,c,c'}\}_{c' \neq c}^C$  is estimated by comparing  $\{\mathcal{P}_g^{m,c,c'}\}_{c' \neq c}^C$  computed from the first data path with  $\mathcal{P}_{sh}^{m,c,c}$  computed from the second path. This method is designed based on an intuitive idea that the shared information distribution  $\mathcal{P}_{sh}^{m,c,c}$  can be regarded as the distribution of the data  $\tilde{\mathcal{X}}^{m,c}$  itself. Therefore, it encompasses the total confusing information of class  $c$  and all the other classes. For any class  $c' \neq c$ , the higher the similarity between the confusing information distribution  $\mathcal{P}_g^{m,c,c'}$  and  $\mathcal{P}_{sh}^{m,c,c}$ , the greater the proportion of confusing information related to  $c'$  in the total confusing information of  $c$ , and thus the higher the degree of confusion between  $c$  and  $c'$ . The estimation of  $\{\beta^{m,c,c'}\}_{c' \neq c}^C$  can be formulated as:

$$\beta^{m,c,c'} = \frac{\exp(-D_{JS}(\mathcal{P}_{sh}^{m,c,c} \parallel \mathcal{P}_g^{m,c,c'}))}{\sum_{t \neq c}^C \exp(-D_{JS}(\mathcal{P}_{sh}^{m,c,c} \parallel \mathcal{P}_g^{m,c,t}))}. \quad (3)$$

$D_{JS}(\cdot \parallel \cdot) \in [0, 1]$  is the Jensen-Shannon Divergence, a measure of the similarity between two probability distributions, with smaller values indicating greater similarity.

4) *Learning Objectives of  $\mathbf{U}^m$* : To learn the two encoders  $\mathbf{E}_{sp}^m$  and  $\mathbf{E}_{sh}^m$  in  $\mathbf{U}^m$ , different loss functions are introduced in two data paths. In the first data path, the loss function  $\mathcal{L}_{gici,1}^m$  is employed to maximize the distance between shared and specific information of each class. Additionally, the reconstruct loss  $\mathcal{L}_{gici,re}^m$  is utilized to further constrain the learned distribution. In the second data path,  $\mathcal{L}_{gici,2}^m$  is used to ensure the distribution  $\mathcal{P}_{sh}^{m,c,c}$  contains all the information in  $\tilde{\mathcal{X}}^{m,c}$ . Furthermore, the constrain  $\mathcal{L}_{gici}^{sym,m}$  that minimize the difference between  $\mathcal{P}_{sp}^{m,c,c'}$  and  $\mathcal{P}_g^{m,c',c}$  is designed to ensure

the symmetric of the learned *ICI*.  $\mathcal{L}_{gici,1}^m, \mathcal{L}_{gici,re}^m, \mathcal{L}_{gici,2}^m$ , and  $\mathcal{L}_{gici}^{sym,m}$  can be formulated as:

$$\begin{aligned} \mathcal{L}_{gici,1}^m &= \frac{1}{C(C-1)} \sum_c \sum_{c'} -D_{JS}(\mathcal{P}_{sh}^{m,c,c'} \parallel \mathcal{P}_{sp}^{m,c,c'}) \\ &\quad - \frac{1}{C(C-1)} \sum_c \sum_{c'} D_{JS}(\mathcal{P}_{sh}^{m,c,c'} \parallel \mathcal{P}_{sp}^{m,c',c}), \\ \mathcal{L}_{gici,re}^m &= \frac{1}{C(C-1)} \sum_c \sum_{c'} \|\mathbf{D}(\tilde{\mathcal{X}}_{sh}^{m,c,c'} + \tilde{\mathcal{X}}_{sp}^{m,c,c'}) - \tilde{\mathcal{X}}^{m,c}\|_2 \\ &\quad + \frac{1}{C(C-1)} \sum_c \sum_{c'} \|\mathbf{D}(\tilde{\mathcal{X}}_{sh}^{m,c,c'} + \tilde{\mathcal{X}}_{sp}^{m,c',c}) - \tilde{\mathcal{X}}^{m,c'}\|_2, \\ \mathcal{L}_{gici,2}^m &= \frac{1}{C} \sum_c -\log \mathcal{P}_g^{m,c,c}(\tilde{\mathcal{X}}^{m,c}), \\ \mathcal{L}_{gici}^{sym,m} &= \frac{1}{C(C-1)} \sum_c \sum_{c'} D_{JS}(\mathcal{P}_{sp}^{m,c,c'} \parallel \mathcal{P}_{sp}^{m,c',c}). \end{aligned} \quad (4)$$

$\mathbf{D}$  is the decoder,  $\tilde{\mathcal{X}}_{sh}^{m,c,c'}$ ,  $\tilde{\mathcal{X}}_{sp}^{m,c,c'}$ , and  $\tilde{\mathcal{X}}_{sp}^{m,c',c}$  refers to samples resampled from the distribution  $\mathcal{P}_{sh}^{m,c,c'}$ ,  $\mathcal{P}_{sp}^{m,c,c'}$ , and  $\mathcal{P}_{sp}^{m,c',c}$ , respectively. All the  $\mathbf{U}^m$  in **GICI** is trained by minimizing the total loss  $\mathcal{L}_{gici}$  formulated as:

$$\mathcal{L}_{gici} = \frac{1}{M} \sum_m (\mathcal{L}_{gici,1}^m + \mathcal{L}_{gici,re}^m + \mathcal{L}_{gici,2}^m + \mathcal{L}_{gici}^{sym,m}). \quad (5)$$

### C. Global-Guided Sample ICI Learning (SICI)

1) *Feature Extraction*: For each input sample  $x_i = \{x_i^m \in \mathbb{R}^{d^m}\}_{m=1}^M$  in  $\mathcal{D} = (\mathcal{X}, \mathcal{Y})$ ,  $M$  modality-specific encoders  $\mathbf{E} = \{\mathbf{E}^m\}_{m=1}^M$  are employed to separate the discriminative features and *ICI* from each modality's feature. The feature separation is designed based on the observation that given a high-dimensional feature vector, only a subset of features are informative and relevant to the class label [16], [18], [47], [50]. Those informative features are regarded as discriminative, while the others are redundant. Specifically, for the  $m$ -th modality, the encoder  $\mathbf{E}^m$  takes the input feature vector  $x_i^m$  and learns a corresponding feature informativeness mask  $w_i^m \in \mathbb{R}^{d^m}$ :

$$w_i^m = \mathbf{E}^m(x_i^m). \quad (6)$$

Each element of  $w_i^m \in \mathbb{R}^{d^m}$  represents the informativeness of each feature value in the feature vector  $x_i^m$ . Subsequently, the learned informativeness mask  $w_i^m$  is element-wise multiplied with the input sample  $x_i^m$  to obtain discriminative features  $h_i^m$ , while its complement is element-wise multiplied with  $x_i^m$  to obtain *ICI* $_i^m$ . The calculation is formulated as follows:

$$\begin{aligned} h_i^m &= x_i^m \odot w_i^m, \\ ICI_i^m &= x_i^m \odot (1 - w_i^m). \end{aligned} \quad (7)$$

2) *Global-Level ICI Elimination*: Under the supervision of the ground-truth label, the informativeness mask  $w_i^m$  has removed some of the redundant features from  $h_i^m$ . The global *ICI* distribution learned by **GICI** is utilized to guide the thorough removal of global-level *ICI* from  $h_i^m$  to enhance its

reliability further. Specifically, the distance between  $\{h_i^m\}_{m=1}^M$  and global *ICI* distribution  $\mathcal{P}_g$  is maximized, which can be achieved by minimizing  $\mathcal{L}_{sici}$ :

$$\mathcal{L}_{sici} = \frac{1}{N} \frac{1}{M} \sum_i \sum_m \log \mathcal{P}_g^{m, y_i}(h_i^m). \quad (8)$$

$y_i$  is the label of the sample  $x_i$ .  $\mathcal{P}_g^{m, y_i}(\cdot)$  refers to the posterior probability of an input on  $\mathcal{P}_g^{m, y_i}$ , which can be calculated as:

$$\mathcal{P}^{m, y_i}(x) = \sum_{c \neq y_i}^C \beta^{m, y_i, c} \cdot \mathcal{P}^{m, y_i, c}(x). \quad (9)$$

#### D. Sample-Adaptive Cross-modality Information Compensation (CMIC)

After the global-level *ICI* is removed in the discriminative feature  $\{h_i^m\}_{m=1}^M$  for the input sample  $x_i$ , the proposed **CMIC** further eliminates the individual-level *ICI*. As analyzed in Section I, the individual *ICI* introduces varying information incompleteness and quality across modalities in different samples. Therefore, **CMIC** designs a cross-modality information compensation method in a sample-adaptive way. Specifically, it first achieves interpretable cross-modality compensatory information query based on the complementary relationship between  $\{h_i^m\}_{m=1}^M$  and  $\{ICI_i^m\}_{m=1}^M$  across modalities. Furthermore, the discriminative feature of each modality is adaptively enhanced with the compensatory information from all the other modalities. The relative discriminative power is proposed to integrate compensatory information from modalities based on their relative qualities, thereby promoting the reliability of modality enhancement.

1) *Cross-Modality Compensatory Information Query*: As shown in Equation 7,  $h_i^m$  and  $ICI_i^m$  are complementary for a certain modality  $m$ . Therefore, it is a feasible way to obtain information that  $h_i^m$  lacks from the discriminative features  $h_i^{m'}$  of other modalities  $m'$  using  $ICI_i^m$ . To this end, a cross-modality attention mechanism is employed to query compensatory information from discriminative feature  $h_i^{m'}$  of each of the other modalities  $m'$ , ( $m' \neq m, m' \in [1, M]$ ) for  $h_i^m$  based on  $ICI_i^m$ , which can be formulated as:

$$\begin{aligned} \mathbf{Q}_i^m &= W_Q(ICI_i^m), \quad \forall m \in [1, M], \\ \mathbf{K}_i^{m'} &= W_K(h_i^{m'}), \quad \forall m' \in [1, M], m' \neq m, \\ \mathbf{V}_i^{m'} &= W_V(h_i^{m'}), \quad \forall m' \in [1, M], m' \neq m. \\ A_i^{m \leftarrow m'} &= \text{Softmax}\left(\frac{\mathbf{Q}_i^m (\mathbf{K}_i^{m'})^T}{\sqrt{d}}\right). \\ \mathbf{z}_i^{m \leftarrow m'} &= A_i^{m \leftarrow m'} \mathbf{V}_i^{m'}. \end{aligned} \quad (10)$$

$W_Q, W_K, W_V$  are three learnable mappings that project  $ICI_i^m$  and discriminative features of one of the other modalities  $h_i^{m'}$  into the query, key, and value matrix.  $A_i^{m \leftarrow m'}$  is the attention map.  $\mathbf{z}_i^{m \leftarrow m'}$  is the compensatory information queried from modality  $m'$  for modality  $m$ .  $\mathbf{Z}_i^{m \leftarrow} = \{\mathbf{z}_i^{m \leftarrow m'}\}_{m' \neq m}^M$  is the compensation information obtained by the  $m$ -th modality from other modalities  $m'$ .

2) *Modality Enhancement Based On Relative Discriminative Power*: To ensure the reliability of modality enhancement using the queried compensatory information from other modalities, this work proposes to assess the relative discriminative power between modalities. Modalities with relatively higher quality should have a greater contribution to the enhancement. To estimate the quality of each modality, a method that considers global and individual-level noise is first employed. Specifically, the mutual information is first utilized to compute the informativeness of each feature of a certain modality  $m$  at the global level, which can be formulated as:

$$I^m = \frac{2 \times I(\mathcal{X}^m, \mathcal{Y})}{H(\mathcal{X}^m) + H(\mathcal{Y})} \in \mathbb{R}^{d^m}. \quad (11)$$

$\mathcal{X}^m = \{\mathbf{x}_i^m\}_{i=1}^N$  represents all samples from the  $m$ -th modality,  $I(\cdot, \cdot)$  is the mutual information calculation,  $H(\cdot)$  is the entropy of a variable. Then, the feature informativeness at the individual level learned by the informativeness mask  $w_i^m$  in the **SICI** module is integrated into the global-level informativeness estimation  $I^m$ . The discriminative power of the feature vector  $h_i^m$  retained after masking by  $w_i^m$  is estimated by measuring the consistency between  $w_i^m$  and  $I^m$ :

$$\begin{aligned} \delta_i^m &= -|w_i^m - I^m| \in \mathbb{R}^{d^m}. \\ D_i^m &= \sigma(W^{m+}(\delta_i^m)) = \sigma(\exp(\theta) \cdot \delta_i^m). \end{aligned} \quad (12)$$

$|\cdot|$  denotes the element-wise absolute value of the vector.  $W^{m+}$  is a learnable positive mapping that maps  $\delta_i^m$  to the discriminative power estimation value  $D_i^m$ .  $\sigma(\cdot)$  is the sigmoid function,  $\exp(\cdot)$  denotes the exponential function that reparameterize the learnable parameter  $\theta$  to ensure the positive mapping. Subsequently, the relative discriminative power  $k_i^{m \leftarrow m'}$  between modality  $m$  and other modalities  $m'$  can be calculated by:

$$k_i^{m \leftarrow m'} = \frac{\exp(\frac{D_i^{m'}}{D_i^m})}{\sum_{n \neq m}^M \exp(\frac{D_i^n}{D_i^m})}. \quad (13)$$

After the relative discriminative power  $k_i^{m \leftarrow} = \{k_i^{m \leftarrow m'}\}_{m' \neq m}^M$  is estimated, the compensatory information  $\mathbf{Z}_i^{m \leftarrow} = \{\mathbf{z}_i^{m \leftarrow m'}\}_{m' \neq m}^M$  is aggregated with weights of  $k_i^{m \leftarrow} = \{k_i^{m \leftarrow m'}\}_{m' \neq m}^M$  and used to enhance the discriminative feature  $h_i^m$  of the  $m$ -th modality:

$$f_i^m = h_i^m + \sum_{m' \neq m}^M k_i^{m \leftarrow m'} \cdot \mathbf{z}_i^{m \leftarrow m'}. \quad (14)$$

$f_i = \{f_i^m\}_{m=1}^M$  is the enhanced feature of the input sample  $x_i = \{x_i^m\}_{m=1}^M$  with both modality-specific and cross-modality noise removed. The reliable classification result  $\hat{y}_i$  of the sample  $x_i$  is obtained by  $\hat{y}_i = \text{Classifier}(\text{Concat}(\{f_i^m\}_{m=1}^M))$ .

#### E. Learning of MICINet

In addition to  $\mathcal{L}_{gici}$  (Equation 5) and  $\mathcal{L}_{sici}$  (Equation 8), the training of MICINet also incorporates a loss function  $\mathcal{L}_{align}$

TABLE I

COMPARISON OF CLASSIFICATION PERFORMANCE BETWEEN THE PROPOSED MICINET AND OTHER RELIABLE MULTIMODAL CLASSIFICATION METHODS ON THE BRCA, ROSMAP, CUB, AND UPMC FOOD101 DATASETS UNDER DIFFERENT NOISE SETTINGS. THE BEST RESULTS UNDER VARIOUS NOISE SETTINGS ARE INDICATED IN BOLD, WHILE THE SECOND-BEST RESULTS ARE UNDERLINED.

Data Type	Methods	BRCA			ROSMAP			CUB			FOOD101		
		ACC	WeightedF1	MacroF1	ACC	F1	AUC	ACC	WeightedF1	MacroF1	ACC	WeightedF1	MacroF1
$\eta = 0$ $\epsilon = 0$	MD [16]	83.7	83.6	79.9	83.0	83.0	90.2	91.9	92.0	91.9	92.3	92.7	92.7
	MLCLNet [47]	82.3	82.2	78.6	79.4	79.2	89.3	90.2	90.3	89.9	92.1	92.2	92.1
	QMF [19]	82.5	82.3	79.1	78.3	78.1	85.1	88.3	88.3	87.9	91.7	92.2	92.1
	PDF [20]	82.1	81.7	76.4	80.2	82.9	87.1	89.2	89.1	88.9	92.2	92.4	92.3
	NCR [22]	77.9	75.3	71.1	79.2	80.0	87.4	83.9	83.7	84.0	91.1	91.5	91.5
	ALBEF [23]	78.2	75.2	71.3	79.0	80.3	86.5	84.0	84.2	84.2	91.2	91.5	91.4
	SMILE [28]	80.5	81.0	78.2	79.2	79.5	87.4	88.6	88.6	88.3	91.3	91.7	91.6
	MICINet	<b>85.6</b>	<b>85.7</b>	<b>82.4</b>	<b>87.7</b>	<b>88.1</b>	<b>93.2</b>	<b>92.8</b>	<b>92.8</b>	<b>92.6</b>	<b>93.2</b>	<b>93.4</b>	<b>93.2</b>
$\eta = 0$ $\epsilon = 1$	MD [16]	78.3	77.4	69.0	75.5	79.0	83.2	90.1	90.1	90.2	92.2	92.5	92.4
	MLCLNet [47]	77.0	76.6	70.8	74.1	78.5	82.5	86.4	86.5	86.3	88.7	88.5	88.7
	QMF [19]	76.4	75.8	71.0	70.8	75.0	78.9	86.5	86.5	86.4	91.2	91.7	91.7
	PDF [20]	76.0	73.6	67.4	68.9	73.6	78.6	88.2	88.2	88.2	89.2	90.1	90.1
	NCR [22]	71.5	66.8	53	67.9	71.7	70.4	82.0	81.8	81.9	88.0	89.1	89.1
	ALBEF [23]	71.2	66.5	52.6	68.2	71.9	70.6	81.7	81.8	81.8	87.6	88.4	88.3
	SMILE [28]	71.5	67.0	54.3	67.6	72.3	71.1	82.0	81.9	81.9	89.7	90.1	90.0
	MICINet	<b>84.4</b>	<b>84.0</b>	<b>80.0</b>	<b>81.1</b>	<b>81.1</b>	<b>85.6</b>	<b>92.8</b>	<b>92.8</b>	<b>92.6</b>	<b>93.0</b>	<b>93.1</b>	<b>93.1</b>
$\eta = 20\%$ $\epsilon = 0$	MD [16]	72.6	69.7	54.5	72.6	73.9	78.1	69.4	69.3	68.3	74.1	74.2	74.2
	MLCLNet [47]	70.4	68.2	50.5	70.4	70.6	76.2	69.2	68.8	68.1	73.2	73.9	74.0
	QMF [19]	68.8	64.9	50.3	70.8	69.3	73.1	70.3	70.2	69.5	73.4	74.3	74.3
	PDF [20]	65.0	56.7	41.7	67.9	72.8	77.3	69.4	69.3	69.0	74.1	74.2	74.2
	NCR [22]	69.6	65.4	51.1	69.8	70.9	76.3	71.6	71.2	71.9	73.9	74.4	74.4
	ALBEF [23]	69.1	65.2	50.8	70.0	73.1	77.6	71.5	71.2	71.8	74.0	74.2	74.2
	SMILE [28]	68.9	64.6	50.2	69.1	70.0	77.4	62.2	62.3	61.9	73.2	73.4	73.4
	MICINet	<b>73.4</b>	<b>73.0</b>	<b>69.4</b>	<b>79.2</b>	<b>79.6</b>	<b>83.5</b>	<b>73.0</b>	<b>73.3</b>	<b>72.6</b>	<b>75.5</b>	<b>75.6</b>	<b>75.6</b>
$\eta = 20\%$ $\epsilon = 1$	MD [16]	65.8	58.5	42.4	68.9	72.7	72.3	68.5	67.9	67.2	73.3	73.4	73.4
	MLCLNet [47]	65.1	58.2	42.1	64.9	70.1	71.5	67.6	67.7	68.3	72.9	72.8	73.1
	QMF [19]	65.0	58.9	44.4	62.2	69.2	70.1	64.8	65.1	64.8	73.2	73.7	73.7
	PDF [20]	60.5	48.1	31.0	66.0	72.7	72.1	68.5	68.0	67.8	72.2	72.9	72.9
	NCR [22]	68.1	66.2	48.2	68.9	70.3	68.0	70.5	70.1	71.0	72.0	72.8	72.8
	ALBEF [23]	67.9	66.0	48.3	69.2	72.1	72.2	70.0	70.2	70.6	72.8	73.4	73.2
	SMILE [28]	66.8	65.9	47.8	68.4	68.9	70.2	56.8	56.4	55.9	70.8	71.3	71.2
	MICINet	<b>69.2</b>	<b>67.9</b>	<b>60.1</b>	<b>76.4</b>	<b>78.6</b>	<b>77.2</b>	<b>73.0</b>	<b>73.0</b>	<b>72.4</b>	<b>75.3</b>	<b>75.1</b>	<b>75.2</b>

that constrains sample feature alignment, as well as an overall classification loss  $\mathcal{L}_{task}$ , which can be formulated as:

$$\mathcal{L}_{align} = \frac{1}{NM(M-1)} \sum_{i=1}^N \sum_{m=1}^M \sum_{m' \neq m}^M (f_i^m)^T \cdot f_i^{m'},$$

$$\mathcal{L}_{task} = \sum_{i=1}^N CrossEntropy(\hat{y}_i, y_i). \quad (15)$$

$T$  refers to the transpose of the feature vector. MICINet is trained by minimizing the total loss  $\mathcal{L}$ :

$$\mathcal{L} = \mathcal{L}_{gici} + \mathcal{L}_{sici} + \mathcal{L}_{task} - \mathcal{L}_{align}. \quad (16)$$

#### IV. EXPERIMENTS

This section presents experiments that comprehensively validate the effectiveness of the proposed MICINet in removing both modality-specific and cross-modality noise. Several reliable multimodal classification methods are introduced to demonstrate the improvement of MICINet. In the following sections, the experimental settings are first elaborated in Section IV-A. Subsequently, the main questions to be verified are highlighted in Section IV-B.

##### A. Experimental Settings

1) *Datasets*: Experiments are conducted on four commonly used multimodal datasets from different tasks including biomedical classification and image-text classification tasks.

- **BRCA**: BRCA [51] is a dataset for breast invasive carcinoma PAM50 subtype classification. The dataset comprises 875 samples, with each sample containing features from three modalities: mRNA expression data (mRNA), DNA methylation data (meth), and miRNA expression data (miRNA). These samples are categorized into five subtypes: Normal-like, Basal-like, HER2-enriched, Luminal A, and Luminal B, with 115, 131, 46, 435, and 147 samples respectively. BCRA can be obtained from The Cancer Genome Atlas program (TCGA) <sup>1</sup>.
- **ROSMAP**: ROSMAP [52]–[54] is a dataset containing samples from Alzheimer’s patients and normal control subjects. The dataset consists of 351 samples, including 182 Alzheimer’s disease patients and 169 normal control samples. Each sample includes data from three modalities: mRNA expression data (mRNA), DNA methylation data (meth), and miRNA expression data (miRNA).
- **CUB**: Caltech-UCSD Birds dataset [55] comprises 200 categories of birds. It contains a total of 11,788 samples, with each sample including data from two modalities: images of birds and their corresponding textual descriptions.
- **UPMC FOOD101**: The UPMC FOOD101 dataset [56] comprises food images from 101 categories obtained through Google Image search and corresponding textual descriptions. This dataset contains 90,704 samples, where

<sup>1</sup><https://www.cancer.gov/aboutnci/organization/ccg/research/structuralgenomics/tcga>

TABLE II

ABLATION STUDY OF DIFFERENT COMPONENTS OF THE PROPOSED MICINET ON THE BRCA, ROSMAP, CUB, AND UPMC FOOD101 DATASETS. THE BEST RESULTS ARE HIGHLIGHTED IN BOLD.

Data Type	Methods			BRCA			ROSMAP			CUB			FOOD101		
	SICI	CMIC	RDP	ACC	WeightedF1	MacroF1	ACC	F1	AUC	ACC	WeightedF1	MacroF1	ACC	WeightedF1	MacroF1
$\eta = 20\%$ $\epsilon = 0$	X	X	X	59.7	47.3	30.2	71.7	74.1	78.1	71.2	71.1	70.3	72.1	72.5	72.5
	✓	X	X	71.5	70.2	64.6	74.5	74.8	79.6	72.3	72.4	71.7	73.4	73.5	73.5
	✓	✓	X	72.4	72.1	67.8	78.3	78.9	81.7	<b>73.0</b>	72.7	72.0	74.8	74.7	74.7
	✓	✓	✓	<b>73.4</b>	<b>73.0</b>	<b>69.4</b>	<b>79.2</b>	<b>79.6</b>	<b>83.5</b>	<b>73.0</b>	<b>73.3</b>	<b>72.6</b>	<b>75.5</b>	<b>75.6</b>	<b>75.6</b>
$\eta = 0$ $\epsilon = 1$	X	X	X	67.6	33.1	13.3	67.9	73.0	76.4	84.7	84.8	84.7	84.5	84.2	84.3
	✓	X	X	74.8	41.6	23.6	74.5	77.7	83.1	91.0	91.0	90.6	90.6	90.5	90.3
	✓	✓	X	82.5	82.3	78.9	80.2	<b>81.7</b>	85.0	92.0	91.9	91.9	92.2	92.1	92.1
	✓	✓	✓	<b>84.4</b>	<b>84.0</b>	<b>80.0</b>	<b>81.1</b>	81.1	<b>86.5</b>	<b>92.8</b>	<b>92.8</b>	<b>92.6</b>	<b>93.0</b>	<b>93.1</b>	<b>93.1</b>
$\eta = 20\%$ $\epsilon = 1$	X	X	X	67.0	31.8	12.5	48.5	48.3	51.2	70.3	70.2	69.7	70.2	70.5	70.6
	✓	X	X	67.7	64.5	50.0	68.3	68.5	72.6	72.0	72.1	72.0	73.2	73.2	73.2
	✓	✓	X	69.0	66.8	59.4	75.5	76.0	76.5	72.4	72.3	72.0	74.4	74.5	74.4
	✓	✓	✓	<b>69.2</b>	<b>67.9</b>	<b>60.1</b>	<b>76.4</b>	<b>78.6</b>	<b>77.2</b>	<b>73.0</b>	<b>73.0</b>	<b>72.4</b>	<b>75.3</b>	<b>75.1</b>	<b>75.2</b>

each sample’s image and text are collected from uncontrolled environments, thus inherently containing noise.

2) *Compared Methods:*

a) *Modality-Specific Noise Removal Methods:* Several state-of-the-art methods capable of reliable classification on multimodal data with modality-specific noise are introduced, including multimodal dynamics (MD) [16], multi-level confidence learning (MLCLNet) [47], quality-aware multimodal fusion (QMF) [19], and predictive dynamic fusion (PDF) [20].

b) *Cross-Modality Noise Removal Methods:* Several representative approaches from this field are compared in the experiments, including Noisy Correspondence Rectifier (NCR) [22], Align before Fuse (ALBEF) [23], and Semantic Invariance Learning (SMILE) [28].

3) *Evaluation Metrics:*

a) *BRCA & CUB & UPMC FOOD101:* BRCA, CUB and UPMC FOOD101 provide multi-class classification task. Three metrics, including accuracy (ACC), average F1 score weighted by support (WeightedF1), and macro-averaged F1 score (MacroF1), are employed to evaluate the performance of different methods.

b) *ROSMAP:* ROSMAP provides binary classification task. The accuracy (ACC), F1 score (F1), and area under the receiver operating characteristic curve (AUC) of different methods are reported by experiment.

4) *Implementation Details:*

a) *Training Details:* We implement the proposed method and other comparing methods on the PyTorch 1.12.0 and cuda 11.6 platform, running on Ubuntu 20.04.2 LTS, utilizing one GPU (NVIDIA RTX A6000 with 48 GB of memory) and CPU of AMD EPYC 75F3. The Adam optimizer with learning rate decay is employed to train the model. The initial learning rate of the Adam optimizer is set to 1e-4, the weight decay is set to 1e-4, and the multiplicative factor of the learning rate decay is set to 0.2. All the quantitative results of the proposed MICINet are the average of five random seeds.

b) *Model Implementation Details:* To evaluate the classification performance of NCR [22] and ALBEF [23], the sample features after being filtered or rectified are utilized to train the classifier. For SMILE [28], the sample features output by its encoders are used to train the classifier.

c) *Experimental Details:* Two types of noise are involved in the experiments: modality-specific and cross-modality

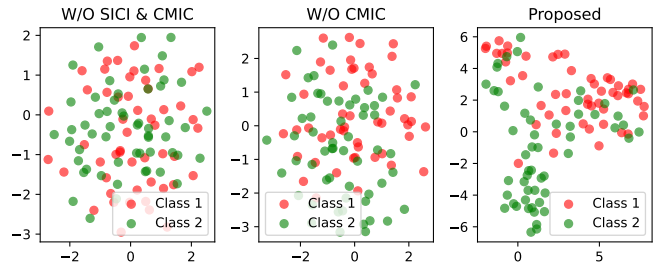


Fig. 2. T-SNE visualizations of sample multimodal features derived from the network with different component combinations under the noise setting of  $\eta = 20\%$ ,  $\epsilon = 5$  on the ROSMAP dataset.

noise. The modality-specific noise is implemented following previous works [15], [17], [20], and  $\epsilon$  is its intensity. The implementation of cross-modality noise follows SMILE [28], where unaligned samples are introduced by shuffling the features of each modality for a random subset of samples with a proportion of  $\eta$ .

B. *Questions To Be Verified*

For clarity, the main questions to be verified in the following experiments are highlighted here:

- RQ1: How does the classification performance and reliability of MICINet compare to other reliable multimodal classification methods under different noise settings?
- RQ2: Do all components of MICINet contribute to achieving reliable classification?
- RQ3: What is the effectiveness of the proposed global ICI learning module (GICI)?
- RQ4: What is the effectiveness of the proposed sample-adaptive cross-modality information compensation module (CMIC)?
- RQ5: Are the two types of noise removed during the learning of MICINet?

V. EXPERIMENTAL RESULTS AND ANALYSIS

This section presents and analyses the experiment results on four datasets and verifies the questions mentioned in Section IV-B.

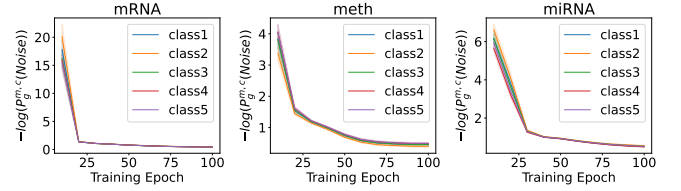
### A. Classification Performance (RQ1)

The classification performance of different methods is evaluated on the BRCA, ROSMAP, CUB, and UPMC FOOD101 datasets under different settings of noise, including “ $\eta = 0, \epsilon = 0$ ”, “ $\eta = 0, \epsilon = 1$ ”, “ $\eta = 20\%, \epsilon = 0$ ”, and “ $\eta = 20\%, \epsilon = 1$ ”. The results are compared in Table I. From the results, the following conclusion can be drawn.

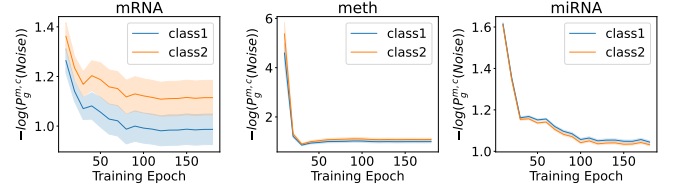
- Cross-modality noise removal methods have limitations in handling modality-specific noise.** Under noise-free or modality-specific noise-only conditions, methods for modality-specific noise removal generally outperform cross-modality noise removal methods. By comparing the results under noise settings “ $\eta = 0, \epsilon = 0$ ” and “ $\eta = 0, \epsilon = 1$ ”, it can be observed that all modality-specific noise removal methods consistently surpass cross-modality noise removal methods on most datasets.
- Modality-specific noise removal methods are less effective at handling cross-modality noise.** With the introduction of cross-modality noise (unaligned samples), the advantage of modality-specific noise removal methods diminishes and is partially surpassed by cross-modality noise removal methods. Comparing the results under noise settings “ $\eta = 20\%, \epsilon = 0$ ” and “ $\eta = 20\%, \epsilon = 1$ ” reveals that cross-modality noise removal methods achieve comparable or superior performance to modality-specific noise removal methods on most datasets.
- MICINet outperforms both modality-specific and cross-modality noise removal methods under all noise settings.** Under the modality-specific noise-only setting (“ $\eta = 0, \epsilon = 1$ ”), MICINet outperforms other state-of-the-art modality-specific noise removal methods. Under the cross-modality noise-only setting (“ $\eta = 20\%, \epsilon = 0$ ”), MICINet outperforms other cross-modality noise removal methods. The possible reason is that MICINet can achieve more reliable noise removal by considering noise at both the global and individual levels. Under the combined conditions of both modality-specific and cross-modality noise (“ $\eta = 20\%, \epsilon = 1$ ”), MICINet outperforms both modality-specific and cross-modality noise removal methods, indicating its capability to more effectively remove both types of noise.

### B. Ablation Study (RQ2)

A comprehensive ablation study is conducted on the four datasets to verify the effectiveness of different components of the proposed MICINet. Specifically, the experiments validate the effectiveness of (1) the global-guided sample *ICI* learning (**SICI**); (2) sample-adaptive cross-modal information compensation (**CMIC**); (3) relative discriminative power (**RDP**) introduced in **CMIC**. The results of the model under different components and data settings are shown in Table II. **SICI** is removed from the model by setting the loss term  $\mathcal{L}_{sici}$  to 0, i.e., the global *ICI* distribution is no longer used to guide the feature learning of samples. **CMIC** is removed by directly performing multimodal fusion on all discriminative power features  $\{h_i^m\}_{m=1}^M$ . **RDP** is removed by setting all



(a) Results on the BRCA dataset.



(b) Results on the ROSMAP dataset.

Fig. 3. Variation of the negative log probability of the added noise in the global *ICI* distribution learned by *GICI* during training on the BRCA and ROSMAP datasets.

TABLE III  
COMPARISON OF RESULTS FOR UNIFORM AND WEIGHTED MIXTURE OF *ICI* DISTRIBUTIONS USING ESTIMATED CONFUSION DEGREE  $\beta$  ON THE ROSMAP DATASET UNDER DIFFERENT NOISE SETTINGS. THE BEST RESULTS ARE HIGHLIGHTED IN BOLD.

Data Type	Method	ACC	F1	AUC
$\eta = 0$ $\epsilon = 0$	uniform mix	83.0	83.3	89.1
	mix with $\beta$	<b>87.7</b>	<b>88.1</b>	<b>93.2</b>
$\eta = 0$ $\epsilon = 1$	uniform mix	75.5	77.0	79.9
	mix with $\beta$	<b>81.1</b>	<b>81.1</b>	<b>85.6</b>
$\eta = 20\%$ $\epsilon = 0$	uniform mix	72.6	73.4	77.8
	mix with $\beta$	<b>79.2</b>	<b>79.2</b>	<b>83.5</b>
$\eta = 20\%$ $\epsilon = 1$	uniform mix	70.8	72.1	70.3
	mix with $\beta$	<b>76.4</b>	<b>78.6</b>	<b>77.2</b>

relative discriminative power values  $\{k_i^{m'}\}_{m' \neq m}^M$  equals to  $\frac{1}{M-1}$ , where  $M$  is the number of modalities.

By comparing the results of different component combinations under “ $\eta = 0, \epsilon = 1$ ” in Table II, one can observe that all three components play a role in enhancing the robustness of MICINet under modality-specific noise. Furthermore, the results of different model versions under “ $\eta = 20\%, \epsilon = 0$ ” demonstrate that all three components contribute to handling cross-modality noise. The results under “ $\eta = 20\%, \epsilon = 1$ ” show that all the components enhance the performance under the coexistence of both two types of noise.

In addition, the experiment conducts t-SNE visualizations of the multimodal features computed by the model under different component combinations. Specifically, the multimodal features of each sample before being fed into the classifier are used for visualization. The results for MICINet without **SICI** and **CMIC**, without only **CMIC**, and the complete MICINet are shown in Figure 2, where the input data is polluted by modality-specific noise of  $\epsilon = 5$  and cross-modality noise of  $\eta = 20\%$ . When **SICI** and **CMIC** are removed, the multimodal features of samples from different classes are largely mixed. As **SICI** and **CMIC** are progressively added,



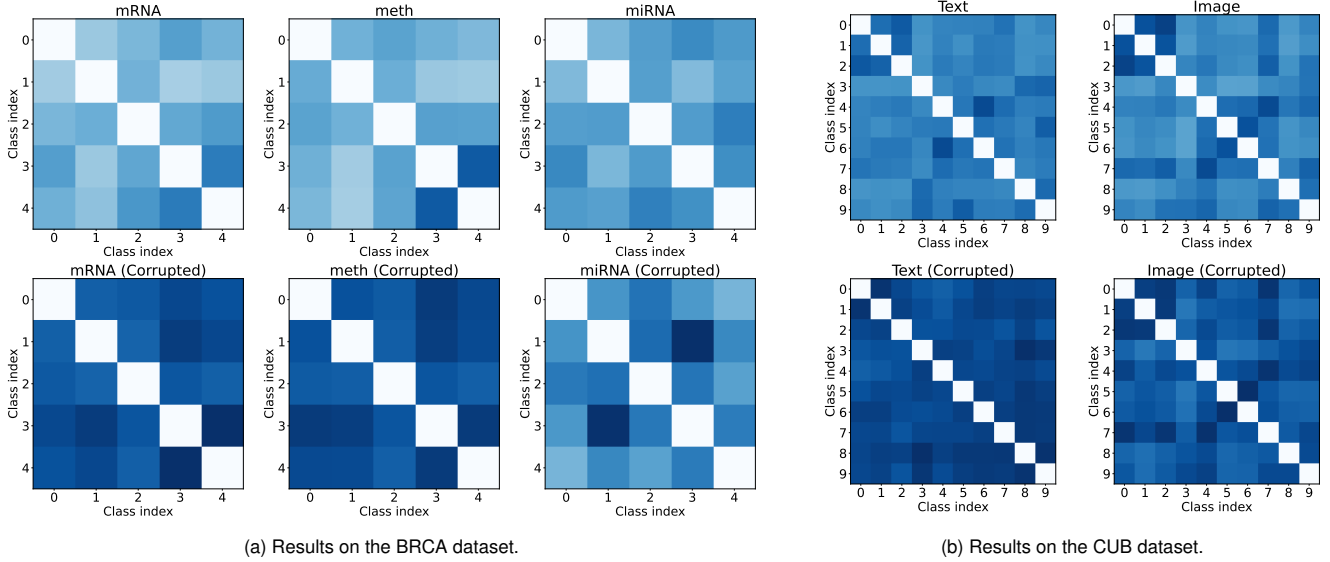


Fig. 4. The visualization results of the inter-class confusion degree estimated by *GICI* in each modality for the BRCA and CUB datasets under noise-free and noise-corrupted settings. For clarity, the CUB dataset only displays the results between the first 10 classes.

the multimodal features of samples from different classes gradually become more separated. This indicates that both *SICI* and *CMIC* contribute to enhancing the discriminative power of sample features and improving noise removal.

### C. The Effectiveness of *GICI* (RQ3)

As elaborated in Section III-B, *GICI* consists of two key processes: learning the *ICI* distribution between different class pairs within each modality  $\{\{\{\mathcal{P}_g^{m,c,c'}\}_{c' \neq c}^C\}_{c=1}^M\}_{m=1}^M$ , and estimating the degree of confusion  $\{\{\{\beta^{m,c,c'}\}_{c' \neq c}^C\}_{c=1}^M\}_{m=1}^M$  between them. The effectiveness of these two processes is validated separately below.

1) *The ICI Distribution Learned in GICI*: Experiments under noise are conducted to investigate whether *GICI* learns the confusing information between different classes. Specifically, modality-specific noise *Noise* with  $\epsilon = 1$  is added to all modalities of all samples in the dataset. At each epoch of the training process, the negative log probability of *Noise* in the distribution  $\mathcal{P}_g^{m,c}$  learned by *GICI* is calculated under each modality and classes:

$$-\log(\mathcal{P}_g^{m,c}(\text{Noise})) = \frac{1}{C} \sum_{c'} -\log(\mathcal{P}_g^{m,c,c'}(\text{Noise})). \quad (17)$$

Figure 3a and 3b show the results on the BRCA and ROSMAP datasets, respectively. The  $-\log(\mathcal{P}_g^{m,c}(\text{Noise}))$  values across all modalities and classes gradually decreased to a lower level with the increase of training epochs. This indicates that *GICI* successfully learned the *ICI* information distribution incorporating noise information.

2) *The Confusion Degree Estimated in GICI*: Extensive experiments are conducted to validate the effectiveness of the inter-class confusion degree estimation method in *GICI*. The estimated inter-class confusion degree  $\beta = \{\{\{\beta^{m,c,c'}\}_{c' \neq c}^C\}_{c=1}^M\}_{m=1}^M$  is visualized under two settings:

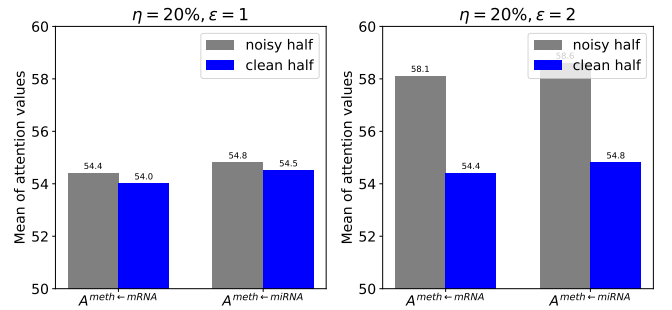


Fig. 5. The mean of attention values corresponds to the noisy and clean halves of the meth feature in attention maps  $A^{\text{meth} \leftarrow \text{mRNA}}$  and  $A^{\text{meth} \leftarrow \text{miRNA}}$ . Noise of “ $\eta = 20\%$ ,  $\epsilon = 1$ ” and “ $\eta = 20\%$ ,  $\epsilon = 2$ ” is added to half of the features only on the meth modality of the ROSMAP dataset. The mean values are amplified by 1000 times for clarity.

without noise and with noise (combination of modality-specific noise with  $\epsilon = 1$  and cross-modality noise with  $\eta = 20\%$ ). Figures 4a and 4b present the results under these two settings on the BRCA and CUB datasets, respectively. Under the noise-free setting (the first row of heatmaps in Figures 4a and 4b), different confusion degrees are exhibited between different class pairs across all modalities. Additionally, each heatmap demonstrated good diagonal symmetry, which indicates the effectiveness of the symmetric constraint  $\mathcal{L}_{gici}^{sym}$  designed in Equation 4. After the data are corrupted by noise (as shown in the second row of heatmaps in Figures 4a and 4b), the confusion degree between all class pairs across all modalities increases. This indicates that the  $\beta = \{\{\{\beta^{m,c,c'}\}_{c' \neq c}^C\}_{c=1}^M\}_{m=1}^M$  estimated in *GICI* can effectively perceive the increased inter-class confusion degree caused by the introduction of noise, ensuring the reliability of the learned global *ICI* distribution.

Additional experiments are conducted to verify the necessity

of mixing  $ICI$  distribution of different class pairs using confusion degree  $\beta = \{\{\{\beta^{m,c,c'}\}_{c' \neq c}^C\}_{c=1}^C\}_{m=1}^M$ . As a comparison, a model version that performs a uniform mixture of  $ICI$  distributions by setting all  $\beta = \frac{1}{C-1}$  is introduced, termed “uniform mix”.  $C$  is the number of classes. Table III compares “uniform mix” with the method that mixes with confusion degree (“mix with  $\beta$ ”). The results show that “mix with  $\beta$ ” outperforms “uniform mix” under various noise conditions. This demonstrates the enhancement of model reliability by mixing the  $ICI$  distributions with the estimated confusion degrees.

#### D. Effectiveness of the CMIC (RQ4)

As demonstrated in Section III-D, **CMIC** consists of two parts: cross-modality compensatory information query and modality enhancement based on relative discriminative power. Extensive experiments are conducted to illustrate the effectiveness of these two parts further.

1) *The Queried Information Among Modalities*: To demonstrate the effectiveness of the cross-modality compensatory information query mechanism, the attention values of cross-modality query attention maps  $A^{m \leftarrow m'}$  are evaluated. Specifically, modality-specific and cross-modality noise is added to half of the features of an arbitrarily selected modality in the dataset. The cross-modality noise is implemented by shuffling the corrupted half of the modality features. The mean of attention values of attention maps for querying compensatory information from the other noise-free modalities is observed under different noise intensities. The results on the ROSMAP dataset are demonstrated in Figure 5, where the noise corruption is applied only on half of the features in the meth modality. The attention maps that meth queries compensatory information from the unaffected modalities (mRNA and miRNA) are denoted as  $A^{meth \leftarrow mRNA}$  and  $A^{meth \leftarrow miRNA}$ , respectively. The attention values corresponding to the noisy half of meth features are higher than those of the clean half under different noise intensities. As noise intensity increases, the attention values for the noisy half also rise, while those for the clean half remain nearly unchanged. The results illustrate that for noise-corrupted features of a certain modality, the attention map can adaptively increase the values according to noise intensity to obtain more compensatory information from discriminative features of other modalities. This indicates that the cross-modality compensatory information query mechanism can interpretably obtain information from other modalities to compensate for the information missing in a modality caused by noise, thereby enhancing the discriminative power across modalities.

2) *Relative Discriminative Power*: Experiment is conducted to explore the responsiveness of relative discriminative power to noise. Specifically, the noise is added to one of the modalities of the dataset, and the relative discriminative power between modalities is investigated. The noise includes cross-modality noise with  $\eta = 20\%$  implemented by shuffling the features of the affected modality in 20% of the samples. Also, the modality-specific noise with intensity  $\epsilon$  is added. Figure 6 shows the variation of relative discriminative power

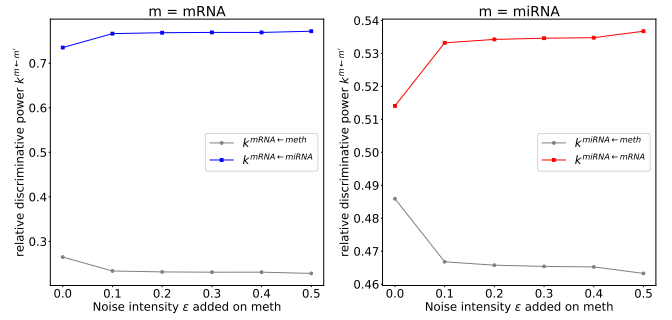


Fig. 6. The relative discriminative power of different modalities as noise with different intensities adds to one of the modalities. The result on the ROSMAP dataset is shown, where noise is added to the meth modality.

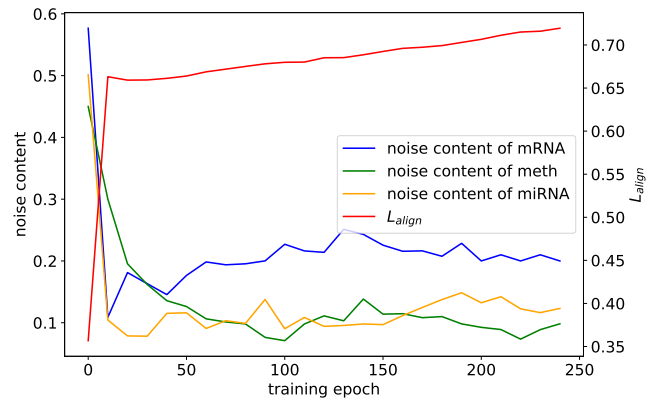


Fig. 7. The removal of modality-specific and cross-modality noise during the training of MICINet.

with increasing  $\epsilon$  on the ROSMAP dataset, where noise is added only to the meth modality. The left subplot shows that when the mRNA modality serves as the query modality, the relative discriminative power  $k^{mRNA \leftarrow meth}$  continuously decreases with increasing noise intensity in the meth modality, while  $k^{mRNA \leftarrow miRNA}$  of the unaffected miRNA modality continuously increases. Similarly, the right subplot shows that when the miRNA modality serves as the query modality, the relative discriminative power  $k^{miRNA \leftarrow meth}$  continuously decreases with increasing noise intensity in the meth modality, while  $k^{miRNA \leftarrow mRNA}$  of the unaffected mRNA modality continuously increases. This indicates that the relative discriminative power can capture the change in relative quality between modalities and enhance the reliability of modality enhancement by relying more on the modalities with higher quality.

#### E. Effectiveness of MICINet in Removing Both Types of Noise (RQ5)

Additional experiments under noise are conducted to verify whether MICINet effectively removed modality-specific and cross-modal noise coexisting in the data. The experiments are performed with modality-specific noise ( $\epsilon = 1$ ) and cross-modality noise ( $\eta = 20\%$ ). The removal of cross-modality

noise in the data is assessed by  $L_{align}$ , which indicates the alignment between modalities. The content of modality-specific noise in the data was measured by the cosine similarity between the features of each modality  $\{f_i^m\}_{i=1}^N$  learned by MICINet and the noise. Figure 7 shows the changes in  $L_{align}$  and the content of modality-specific noise during the training of MICINet on the noisy ROSMAP dataset. It can be seen that while  $L_{align}$  increases to a high level, the content of modality-specific noise in each modality also decreases to a low level. This indicates that MICINet effectively removed both types of noise.

## VI. CONCLUSION

This paper proposes the Multi-Level Inter-Class Confusing Information Removal Network (MICINet) that reliably removes both modality-specific and cross-modality noise at the global and individual levels. Experiments on four datasets have demonstrated that MICINet achieves more robust performance than state-of-the-art reliable multimodal classification methods under various noise conditions and effectively removes both types of noise. The significant role of each proposed component in enhancing the reliability under noise is verified, and their effectiveness is fully validated in extensive experiments. Specifically, experiments have shown that the proposed Global *ICI* learning module (*GICI*) of MICINet effectively learns the inter-class confusion distribution with global noise information and reliably detects changes in inter-class confusion degree caused by noise. Additionally, more experiments have also illustrated the interpretability of the cross-modality compensation information query and the sensitivity of the proposed relative discriminative power to individual-level modality quality changes introduced in the sample-adaptive cross-modality information compensation module (*CMIC*). Despite its effectiveness, MICINet has certain limitations in terms of time complexity, primarily because it learns the global *ICI* distribution through pairwise calculations across classes. Future works will focus on reliable multimodal classification that balances computational efficiency.

## REFERENCES

- [1] C. Zhu, S. Preissl, and B. Ren, "Single-cell multimodal omics: the power of many," *Nature methods*, vol. 17, no. 1, pp. 11–14, 2020.
- [2] A. Baysoy, Z. Bai, R. Satija, and R. Fan, "The technological landscape and applications of single-cell multi-omics," *Nature Reviews Molecular Cell Biology*, vol. 24, no. 10, pp. 695–713, 2023.
- [3] K. Vandereyken, A. Sifrim, B. Thienpont, and T. Voet, "Methods and applications for single-cell and spatial multi-omics," *Nature Reviews Genetics*, vol. 24, no. 8, pp. 494–515, 2023.
- [4] X. Wang, X. Wu, N. Hong, and W. Jin, "Progress in single-cell multimodal sequencing and multi-omics data integration," *Biophysical Reviews*, vol. 16, no. 1, pp. 13–28, 2024.
- [5] D. J. Yeong, G. Velasco-Hernandez, J. Barry, and J. Walsh, "Sensor and sensor fusion technology in autonomous vehicles: A review," *Sensors*, vol. 21, no. 6, p. 2140, 2021.
- [6] K. Huang, B. Shi, X. Li, X. Li, S. Huang, and Y. Li, "Multi-modal sensor fusion for auto driving perception: A survey," *arXiv preprint arXiv:2202.02703*, 2022.
- [7] X. Wang, K. Li, and A. Chehri, "Multi-sensor fusion technology for 3d object detection in autonomous driving: A review," *IEEE Transactions on Intelligent Transportation Systems*, 2023.
- [8] D. Tian, J. Li, and J. Lei, "Multi-sensor information fusion in internet of vehicles based on deep learning: A review," *Neurocomputing*, p. 128886, 2024.
- [9] K. Vinoth and P. Sasikumar, "Multi-sensor fusion and segmentation for autonomous vehicle multi-object tracking using deep q networks," *Scientific Reports*, vol. 14, no. 1, p. 31130, 2024.
- [10] Q. Zhang, Y. Wei, Z. Han, H. Fu, X. Peng, C. Deng, Q. Hu, C. Xu, J. Wen, D. Hu *et al.*, "Multimodal fusion on low-quality data: A comprehensive survey," *arXiv preprint arXiv:2404.18947*, 2024.
- [11] L. Zhang, X. Zhu, X. Chen, X. Yang, Z. Lei, and Z. Liu, "Weakly aligned cross-modal learning for multispectral pedestrian detection," in *Proceedings of the IEEE/CVF international conference on computer vision*, 2019, pp. 5127–5137.
- [12] S. Changpinyo, P. Sharma, N. Ding, and R. Soricut, "Conceptual 12m: Pushing web-scale image-text pre-training to recognize long-tail visual concepts," in *Proceedings of the IEEE/CVF conference on computer vision and pattern recognition*, 2021, pp. 3558–3568.
- [13] Z. Han, C. Zhang, H. Fu, and J. T. Zhou, "Trusted multi-view classification," in *International Conference on Learning Representations*, 2020.
- [14] —, "Trusted multi-view classification with dynamic evidential fusion," *IEEE transactions on pattern analysis and machine intelligence*, vol. 45, no. 2, pp. 2551–2566, 2022.
- [15] Y. Geng, Z. Han, C. Zhang, and Q. Hu, "Uncertainty-aware multi-view representation learning," in *Proceedings of the AAAI Conference on Artificial Intelligence*, vol. 35, no. 9, 2021, pp. 7545–7553.
- [16] Z. Han, F. Yang, J. Huang, C. Zhang, and J. Yao, "Multimodal dynamics: Dynamical fusion for trustworthy multimodal classification," in *Proceedings of the IEEE/CVF conference on computer vision and pattern recognition*, 2022, pp. 20707–20717.
- [17] H. Zhou, Z. Xue, Y. Liu, B. Li, J. Du, M. Liang, and Y. Qi, "Calm: An enhanced encoding and confidence evaluating framework for trustworthy multi-view learning," in *Proceedings of the 31st ACM International Conference on Multimedia*, 2023, pp. 3108–3116.
- [18] X. Zou, C. Tang, X. Zheng, Z. Li, X. He, S. An, and X. Liu, "Dpnet: Dynamic poly-attention network for trustworthy multi-modal classification," in *Proceedings of the 31st ACM International Conference on Multimedia*, 2023, pp. 3550–3559.
- [19] Q. Zhang, H. Wu, C. Zhang, Q. Hu, H. Fu, J. T. Zhou, and X. Peng, "Provable dynamic fusion for low-quality multimodal data," in *International conference on machine learning*. PMLR, 2023, pp. 41753–41769.
- [20] B. Cao, Y. Xia, Y. Ding, C. Zhang, and Q. Hu, "Predictive dynamic fusion," in *Forty-first International Conference on Machine Learning*, 2024. [Online]. Available: <https://openreview.net/forum?id=LYpGLrC4oq>
- [21] F. Radenovic, A. Dubey, A. Kadian, T. Mihaylov, S. Vandenhende, Y. Patel, Y. Wen, V. Ramanathan, and D. Mahajan, "Filtering, distillation, and hard negatives for vision-language pre-training," in *Proceedings of the IEEE/CVF conference on computer vision and pattern recognition*, 2023, pp. 6967–6977.
- [22] Z. Huang, G. Niu, X. Liu, W. Ding, X. Xiao, H. Wu, and X. Peng, "Learning with noisy correspondence for cross-modal matching," *Advances in Neural Information Processing Systems*, vol. 34, pp. 29406–29419, 2021.
- [23] J. Li, R. Selvaraju, A. Gotmare, S. Joty, C. Xiong, and S. C. H. Hoi, "Align before fuse: Vision and language representation learning with momentum distillation," *Advances in neural information processing systems*, vol. 34, pp. 9694–9705, 2021.
- [24] J. Li, D. Li, C. Xiong, and S. Hoi, "Blip: Bootstrapping language-image pre-training for unified vision-language understanding and generation," in *International conference on machine learning*. PMLR, 2022, pp. 12888–12900.
- [25] R. Huang, Y. Long, J. Han, H. Xu, X. Liang, C. Xu, and X. Liang, "Nlip: Noise-robust language-image pre-training," in *Proceedings of the AAAI Conference on Artificial Intelligence*, vol. 37, no. 1, 2023, pp. 926–934.
- [26] X. Li, X. Yin, C. Li, P. Zhang, X. Hu, L. Zhang, L. Wang, H. Hu, L. Dong, F. Wei *et al.*, "Oscar: Object-semantic aligned pre-training for vision-language tasks," in *Computer Vision—ECCV 2020: 16th European Conference, Glasgow, UK, August 23–28, 2020, Proceedings, Part XXXI*. Springer, 2020, pp. 121–137.
- [27] R. Nakada, H. I. Gulluk, Z. Deng, W. Ji, J. Zou, and L. Zhang, "Understanding multimodal contrastive learning and incorporating unpaired data," in *International Conference on Artificial Intelligence and Statistics*. PMLR, 2023, pp. 4348–4380.
- [28] P. Zeng, M. Yang, Y. Lu, C. Zhang, P. Hu, and X. Peng, "Semantic invariant multi-view clustering with fully incomplete information," *IEEE Transactions on Pattern Analysis and Machine Intelligence*, 2023.
- [29] T. Baltrušaitis, C. Ahuja, and L.-P. Morency, "Multimodal machine learning: A survey and taxonomy," *IEEE transactions on pattern analysis and machine intelligence*, vol. 41, no. 2, pp. 423–443, 2018.

- [30] D. Ramachandram and G. W. Taylor, "Deep multimodal learning: A survey on recent advances and trends," *IEEE signal processing magazine*, vol. 34, no. 6, pp. 96–108, 2017.
- [31] Y. Wang, W. Huang, F. Sun, T. Xu, Y. Rong, and J. Huang, "Deep multimodal fusion by channel exchanging," *Advances in neural information processing systems*, vol. 33, pp. 4835–4845, 2020.
- [32] S. Poria, E. Cambria, and A. Gelbukh, "Deep convolutional neural network textual features and multiple kernel learning for utterance-level multimodal sentiment analysis," in *Proceedings of the 2015 conference on empirical methods in natural language processing*, 2015, pp. 2539–2544.
- [33] Y.-H. H. Tsai, S. Bai, P. P. Liang, J. Z. Kolter, L.-P. Morency, and R. Salakhutdinov, "Multimodal transformer for unaligned multimodal language sequences," in *Proceedings of the conference. Association for computational linguistics. Meeting*, vol. 2019. NIH Public Access, 2019, p. 6558.
- [34] L. Hang, Y. Fan, X. Xiaohan *et al.*, "Multi-modal multi-instance learning using weakly correlated histopathological images and tabular clinical information in medical image computing and computer assisted intervention—miccai 2021: 24th international conference, strasbourg, france, september 27–october 1, 2021," *Proceedings, Part VIII*, vol. 24, pp. 529–539 Springer, 2021.
- [35] C. Lee and M. Van der Schaar, "A variational information bottleneck approach to multi-omics data integration," in *International Conference on Artificial Intelligence and Statistics*. PMLR, 2021, pp. 1513–1521.
- [36] D. Kiela, S. Bhooshan, H. Firooz, E. Perez, and D. Testuggine, "Supervised multimodal transformers for classifying images and text," *arXiv preprint arXiv:1909.02950*, 2019.
- [37] Y. Huang, C. Du, Z. Xue, X. Chen, H. Zhao, and L. Huang, "What makes multi-modal learning better than single (provably)," *Advances in Neural Information Processing Systems*, vol. 34, pp. 10944–10956, 2021.
- [38] J. Huang, J. Tao, B. Liu, Z. Lian, and M. Niu, "Multimodal transformer fusion for continuous emotion recognition," in *ICASSP 2020-2020 IEEE International Conference on Acoustics, Speech and Signal Processing (ICASSP)*. IEEE, 2020, pp. 3507–3511.
- [39] R. Hu and A. Singh, "Unit: Multimodal multitask learning with a unified transformer," in *Proceedings of the IEEE/CVF International Conference on Computer Vision*, 2021, pp. 1439–1449.
- [40] D. Hong, L. Gao, N. Yokoya, J. Yao, J. Chanussot, Q. Du, and B. Zhang, "More diverse means better: Multimodal deep learning meets remote-sensing imagery classification," *IEEE Transactions on Geoscience and Remote Sensing*, vol. 59, no. 5, pp. 4340–4354, 2020.
- [41] J. Arevalo, T. Solorio, M. Montes-y Gómez, and F. A. González, "Gated multimodal units for information fusion," *arXiv preprint arXiv:1702.01992*, 2017.
- [42] T. Wang, W. Shao, Z. Huang, H. Tang, J. Zhang, Z. Ding, and K. Huang, "Mogonet integrates multi-omics data using graph convolutional networks allowing patient classification and biomarker identification," *Nature communications*, vol. 12, no. 1, p. 3445, 2021.
- [43] M. Subedar, R. Krishnan, P. L. Meyer, O. Tickoo, and J. Huang, "Uncertainty-aware audiovisual activity recognition using deep bayesian variational inference," in *Proceedings of the IEEE/CVF international conference on computer vision*, 2019, pp. 6301–6310.
- [44] K. Simonyan and A. Zisserman, "Two-stream convolutional networks for action recognition in videos," *Advances in neural information processing systems*, vol. 27, 2014.
- [45] P. Natarajan, S. Wu, S. Vitaladevuni, X. Zhuang, S. Tsakalidis, U. Park, R. Prasad, and P. Natarajan, "Multimodal feature fusion for robust event detection in web videos," in *2012 IEEE Conference on Computer Vision and Pattern Recognition*. IEEE, 2012, pp. 1298–1305.
- [46] M. Federici, A. Dutta, P. Forré, N. Kushman, and Z. Akata, "Learning robust representations via multi-view information bottleneck," in *International Conference on Learning Representations*, 2020. [Online]. Available: <https://openreview.net/forum?id=B1xwcyHFDr>
- [47] X. Zheng, C. Tang, Z. Wan, C. Hu, and W. Zhang, "Multi-level confidence learning for trustworthy multimodal classification," in *Proceedings of the AAAI Conference on Artificial Intelligence*, vol. 37, no. 9, 2023, pp. 11381–11389.
- [48] S. Y. Gadre, G. Ilharco, A. Fang, J. Hayase, G. Smyrnis, T. Nguyen, R. Marten, M. Wortsman, D. Ghosh, J. Zhang *et al.*, "Datacomp: In search of the next generation of multimodal datasets," *Advances in Neural Information Processing Systems*, vol. 36, 2024.
- [49] P. Sharma, N. Ding, S. Goodman, and R. Soicuc, "Conceptual captions: A cleaned, hypernymed, image alt-text dataset for automatic image captioning," in *Proceedings of the 56th Annual Meeting of the Association for Computational Linguistics (Volume 1: Long Papers)*, 2018, pp. 2556–2565.
- [50] X. Zheng, M. Wang, K. Huang, and E. Zhu, "Global and cross-modal feature aggregation for multi-omics data classification and application on drug response prediction," *Information Fusion*, vol. 102, p. 102077, 2024.
- [51] W. Lingle *et al.*, "The cancer genome atlas breast invasive carcinoma collection (tcga-brca)(version 3)[data set]. cancer imag. arch.(2016)."
- [52] S. Mukherjee, S. Walter, J. Kauwe, A. C. in Thought Study Investigators *et al.*, "Religious orders study/memory and aging project investigators; alzheimer's disease genetics consortium," *Genetically predicted body mass index and Alzheimer's disease-related phenotypes in three large samples: Mendelian randomization analyses. Alzheimers Dement*, vol. 11, no. 12, pp. 1439–1451, 2015.
- [53] D. A Bennett, J. A Schneider, Z. Arvanitakis, and R. S Wilson, "Overview and findings from the religious orders study," *Current Alzheimer Research*, vol. 9, no. 6, pp. 628–645, 2012.
- [54] P. De Jager, Y. Ma, C. McCabe, J. Xu, B. Vardarajan, D. Felsky, H. Klein, C. White, M. Peters, B. Lodgson *et al.*, "A multi-omic atlas of the human frontal cortex for aging and alzheimer's disease research. sci data 5: 180142," 2018.
- [55] C. Wah, S. Branson, P. Welinder, P. Perona, and S. Belongie, "The caltech-ucsd birds-200-2011 dataset," 2011.
- [56] X. Wang, D. Kumar, N. Thome, M. Cord, and F. Precioso, "Recipe recognition with large multimodal food dataset," in *2015 IEEE International Conference on Multimedia & Expo Workshops (ICMEW)*. IEEE, 2015, pp. 1–6.